# Characterization of Internal Oxide Layers in 3% Si Grain-Oriented Steel by Electrochemical Methods

*H. Toda, K. Sato, and M. Komatsubara*

**The structure of internal oxide layers in decarburized sheet was studied using a newly developed electrochemical method. Dissolving potential profiles indicated the amount of fayalite ($Fe_2SiO_4$) and silica ($SiO_2$) in the layers. The quantitative data for the contents of fayalite and silica in the internal oxide layers can be easily obtained by this method.**

**Keywords** 3% silicon steel, grain-oriented steel, magnetic steel

## 1. Introduction

Grain-oriented 3% Si steel with a well-defined {110}<001> texture, which is generally called the Goss orientation, is widely used in transformer cores for its superior magnetic properties. The steel is covered with a glass film composed mainly of forsterite ($Mg_2SiO_4$). Forsterite is a reaction product of internal oxides in decarburized steel sheets (primary recrystallized sheets) and MgO coated onto the sheets as an annealing separator prior to secondary recrystallization annealing (Ref 1, 2), and it plays an important role not only in electrical insulation but also in the magnetic properties of the sheets (Ref 3-5). Moreover, it has been reported that the suppression of additional surface oxidation during secondary recrystallization annealing leads secondary recrystallized grains to form more closely in the Goss orientation (Ref 6, 7). It has also been shown that the fayalite content of internal oxide layers has a great effect on secondary recrystallization (Ref 8); secondary recrystallized grains deviate from the Goss orientation as the fayalite content decreases. However, the usual measurement of fayalite content from infrared absorption spectra requires much time because iron must be dissolved and oxides extracted by filtration, and although there have been various studies of the oxidation behavior of Fe-Si alloys (Ref 9-12), only a little work has been done on the composition and structure of the internal oxide layers formed during decarburization annealing.

The purpose of this study was therefore to determine the composition and structure of the internal oxide layers in decarburized sheets by using a convenient electrochemical method.

## 2. Experimental Method

Cold-rolled steel sheets with a thickness of 0.22 mm having the chemical composition shown in Table 1 were decarburized at 820 °C in an atmosphere of 50% $H_2$, 50% $N_2$, and dewpoint of 60 °C. ($P_{H_2O}/P_{H_2}$ ratio of 0.49) under conditions A, B, and C in Table 2.

Surface oxides of the internal oxide layers in these sheets were then identified by infrared reflection spectrum analysis. The oxides extracted from the decarburized sheets were also identified by infrared absorption spectrum analysis.

A scanning electron microscope (SEM) was used to observe the structure of the internal oxide layers at cross-sectional faces of samples that had been polished and etched.

Figure 1 is an outline of the apparatus used in the electrochemical method. Samples for measurement were removed

**Table 1 Chemical composition**

| Element | Composition, mass % |
|---|---|
| Carbon | 0.032 |
| Silicon | 3.37 |
| Manganese | 0.07 |
| Selenium | 0.02 |
| Antimony | 0.025 |
| Iron | bal |

**Table 2 Decarburization annealing condition**

| Specimen | $P_{H_2O}/P_{H_2}$ (Oxygen potential of annealing atmosphere) | Soaking temperature, °C | Soaking time, s |
|---|---|---|---|
| A | 0.49 | 820 | 45 |
| B | 0.49 | 820 | 90 |
| C | 0.49 | 820 | 120 |

**Table 3 Composition of internal oxide layers**

| Specimen | Oxygen amount as fayalite, g/m² | Oxygen amount as silica, g/m² |
|---|---|---|
| A | 0.05 | 1.04 |
| B | 0.12 | 1.05 |
| C | 0.17 | 1.11 |

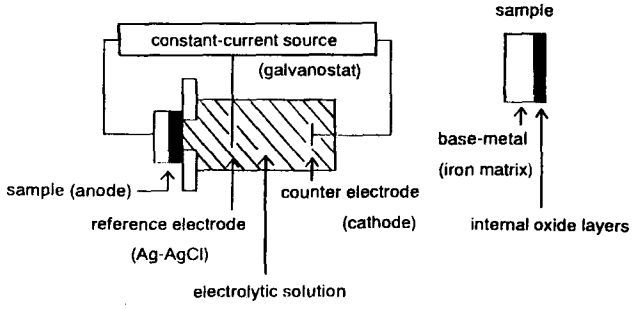


**Fig. 1** Illustration of the apparatus for electrochemical analysis

**H. Toda, K. Sato,** and **M. Komatsubara,** Kawasaki Steel Corp., Iron and Steel Research Lab, 1-Kawasaki-dori, Mizushima, Kurashiki City, Okayama Prefecture, 712 Japan.

from one side of the internal oxide layers and set so that the opposite side was in contact with an electrolytic solution (0.5 mass% NaCl water solution). After the sample surface was set at an anode, a measurement was made under a constant current (75 mA) between the sample and a counterelectrode (Pt-pole; cathode) at room temperature by recording the potential profile (time/voltage curve). A galvanostat was used to maintain a constant current; the distance between the two poles was 110 mm, and the diameter of measurement area was 10 mm. The internal oxide layers were removed from the surface by dissolving iron according to the formula of $Fe \rightarrow Fe^{2+} + 2e^-$ in an anode. The oxide layers at the sample surface had disappeared completely after the measurement for 5 min.

## 3. Results and Discussion

The infrared reflection and absorption spectra of the internal oxides in specimens A, B, and C indicate that the surface oxides of the internal oxide layers are fayalite ($Fe_2SiO_4$), although the main composition of the internal oxide layers themselves is silica ($SiO_2$), as shown in Fig. 2. The amount of fayalite increased in the order A < B < C.

The oxygen amount as fayalite and silica of the internal oxide layers in specimens A, B, and C is shown in Table 3. The oxygen amount as fayalite and silica was calculated from the infrared absorption spectra of oxides using calibration data and the oxygen content of the decarburized sheets.

The surface of the internal oxide layers was covered by fayalite, so this layer was termed the fayalite layer. The SEM photograph in Fig. 3 shows spherical silica mainly in the middle layer of the internal oxide layers, and lamellar silica mainly near the interface between the internal oxide layers and iron matrix. These two layers of spherical silica and lamellar silica are referred to as the silica layer.

Figure 4 shows the potential profiles (time/voltage curve) of specimens A, B, and C after decarburization annealing. The potential profile is described schematically in Fig. 5 in the regions I, II, III, IV, and V. Figure 4 shows that the duration of region I is clearly different and the duration of region III is almost the same among specimens A, B, and C. The meaning of these regions is discussed in the following paragraphs.

In order to identify the material corresponding to each region, the measurement was interrupted at the end of each region. The samples were taken out and investigated by SEM and infrared reflection spectrum analysis.

Electron microscope photographs of decarburized sheets and the sample whose measurement was interrupted immediately after region I are shown in Fig. 6. Figure 6(b) shows that there are two kinds of sites in the sample interrupted after region I. One is covered with spherical particles, which means the fayalite layer has dissolved. The other has a flat surface

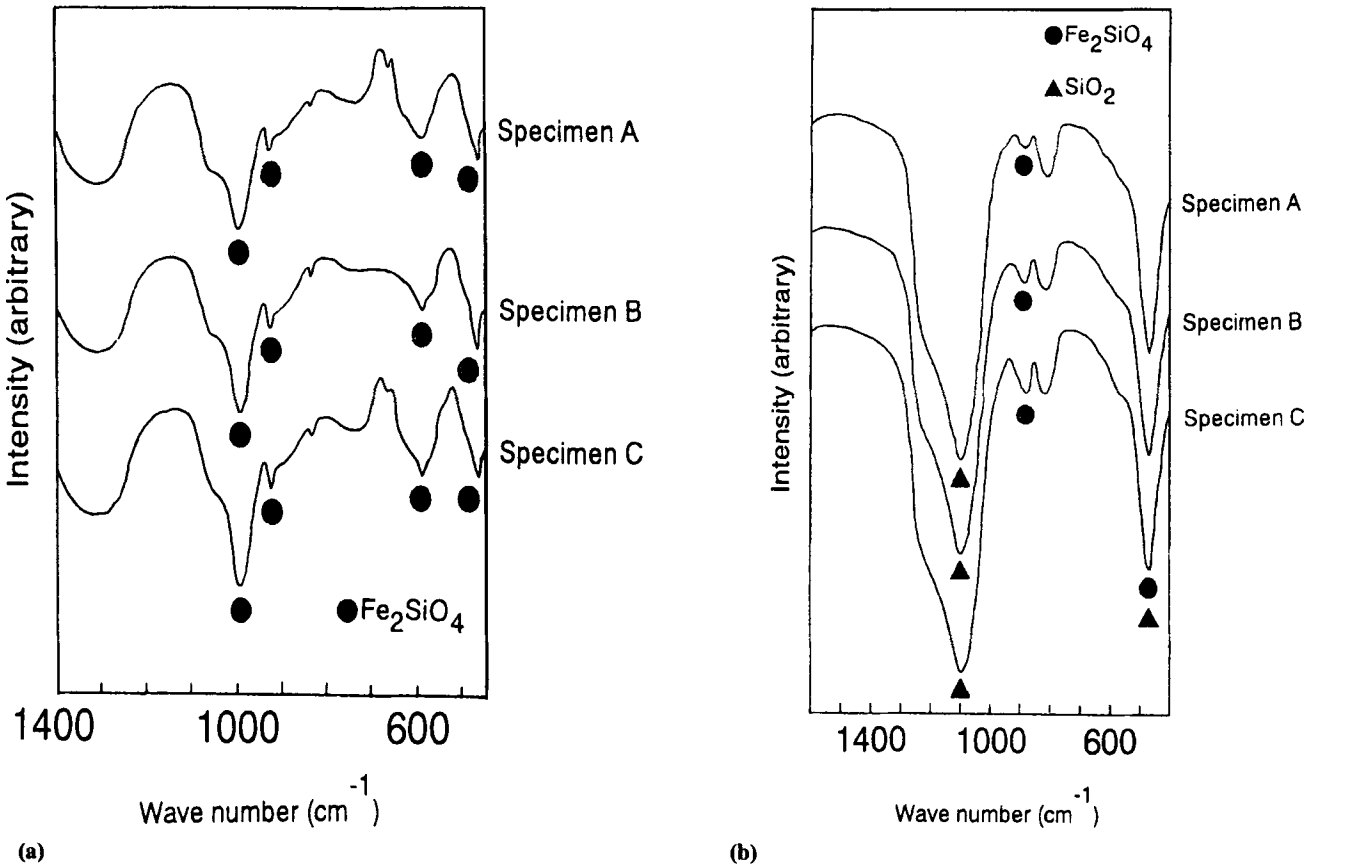


**Fig. 2** Infrared spectra of oxides in the decarburized sheets. (a) Infrared reflection spectra of decarburized sheets. (b) Infrared absorption spectra of oxides extracted from internal oxide layers

with many cracks, which means that the fayalite layer is still present. Therefore, region I reflects the process of dissolution of the fayalite layer; at the end of region II the fayalite layer has dissolved completely.

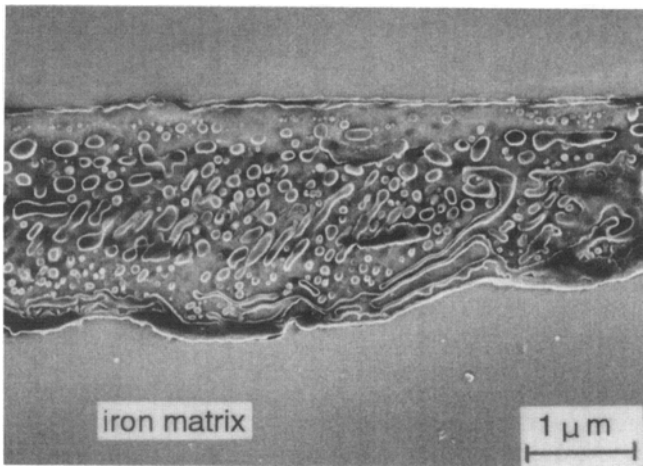


**Fig. 3** Micrograph of cross-sectional structure of internal oxide layers in specimen B by SEM

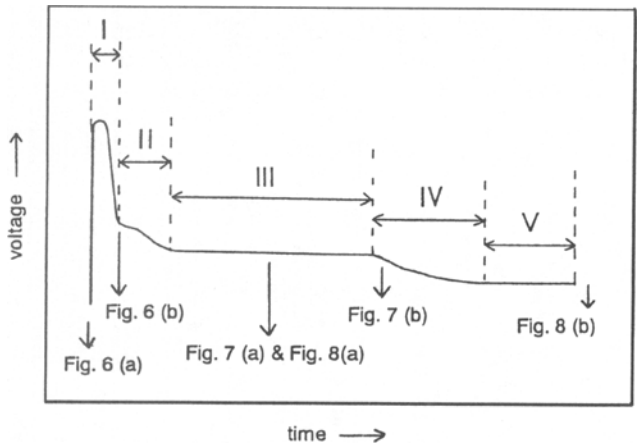


**Fig. 5** Schematic profile with numbered regions of time/voltage curve

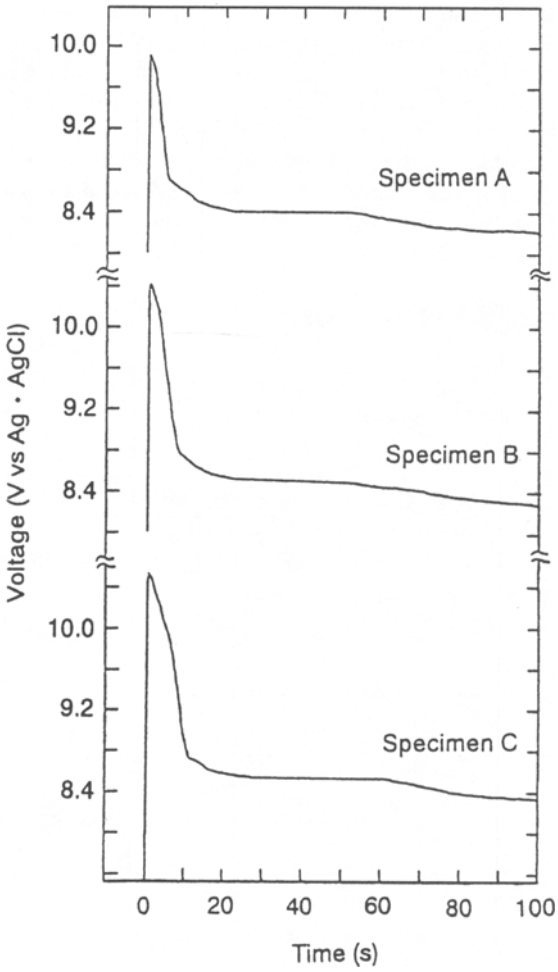


**Fig. 4** Time/voltage curve measured by electrochemical method

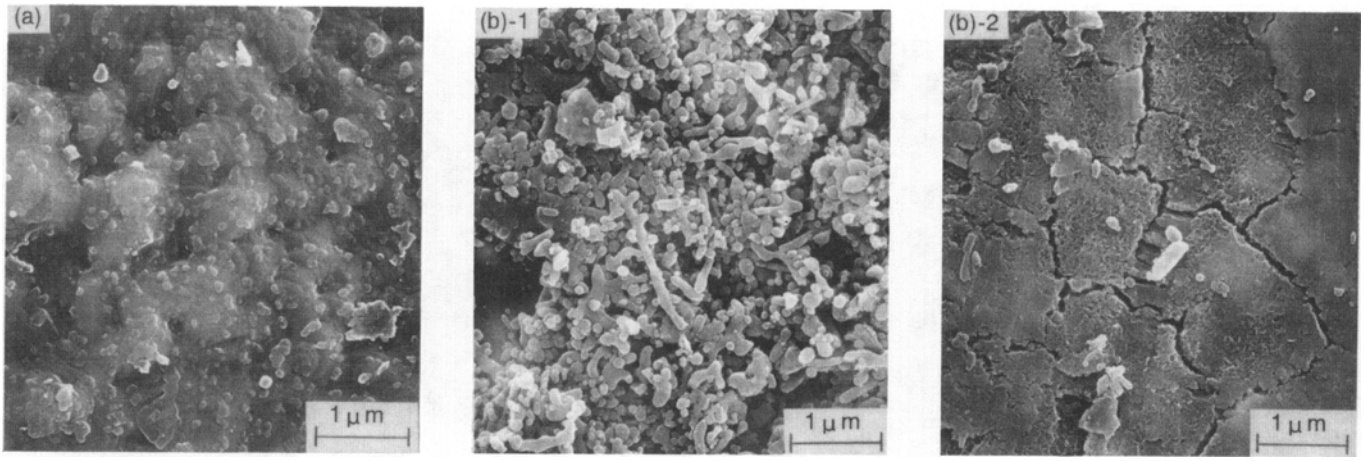


**Fig. 6** Surface features of samples taken out in the middle of electrochemical measurement. (a) SEM micrograph of decarburized sheet. (b) SEM micrographs of sample taken out immediately after region I

Figure 7 shows SEM photographs of the sample interrupted in the middle of region III and the sample interrupted at the beginning of region IV. Figure 7(a) shows that there are two types of particles in the sample surface interrupted in the middle of region III. One is covered with spherical particles and the other with lamellar particles. Crystal facets can also be observed in the sample interrupted at the beginning of region IV, as shown in Fig. 7(b), which means that the silica layer has dissolved and the iron matrix has emerged at the surface. Figure 8 shows the infrared reflection spectra of the sample interrupted in the middle of region III and the sample after measurement for 5 min, which corresponds to region V. Figure 8(a) shows that the sample interrupted in the middle of region III is covered with silica on the surface. Therefore, the spherical particles and lamellar particles shown in Fig. 7(a) are identified as silica. Figure 8(b) shows that the surface state after measurement for 5 min is the iron matrix. Accordingly, region III presents the process of dissolution of the silica layer. At the end of region IV, the silica layer has completely disappeared.

Consequently, the time/voltage curve indicates the process of dissolution of the internal oxide layers. Region I indicates the process of dissolution of the fayalite layer; region III, that of the silica layer; and region V, that of the iron matrix. Region II and region IV are transition regions. Each region of the time/voltage curve can be matched with one of the internal oxide layers, as shown schematically in Fig. 9.

Furthermore, the following various samples were examined by the electrochemical method to obtain the quantitative relationship between the amount of each oxide and the duration of each region. Cold-rolled steel sheets with the composition shown in Table 1 were decarburized at 820 °C in various atmospheres of 50% $H_2$, 50% $N_2$, and the dewpoint of 59 to 61 °C ($P_{H_2O}/P_{H_2}$ ratio of 0.46 to 0.52) for various times (from 45 to 300 s).

The duration of region I shows a good linear relationship with the oxygen amount as fayalite (Fig. 10), while the duration of region III is proportional to the oxygen amount as silica (Fig. 11). These results show that quantitative data for the con-

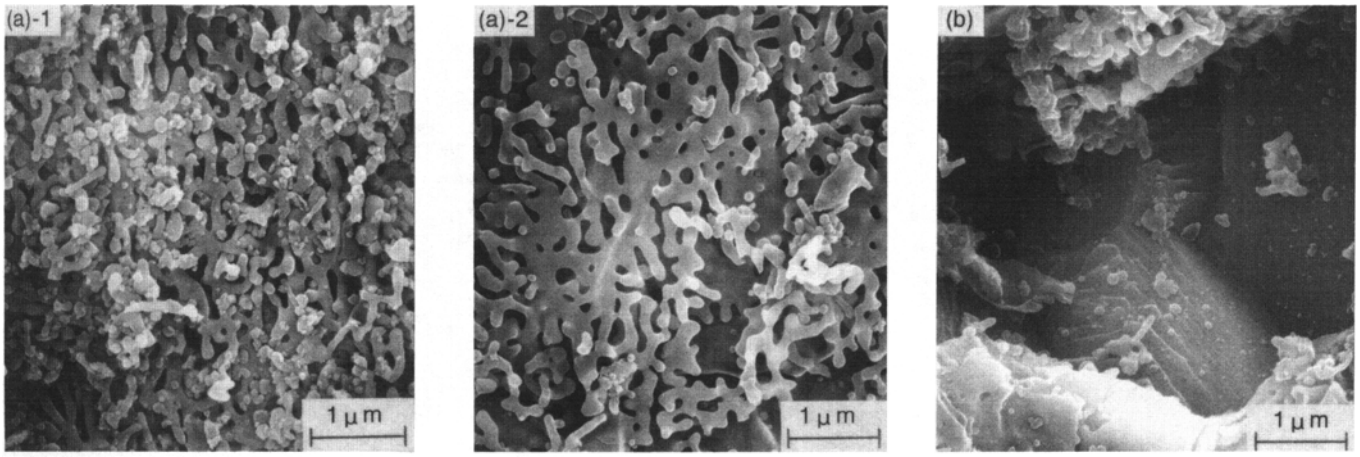


**Fig. 7** Surface features of samples taken out in the middle of electrochemical measurement. (a) SEM micrographs of sample taken out in the middle of region III. (b) SEM micrograph of sample taken out at the beginning of region IV

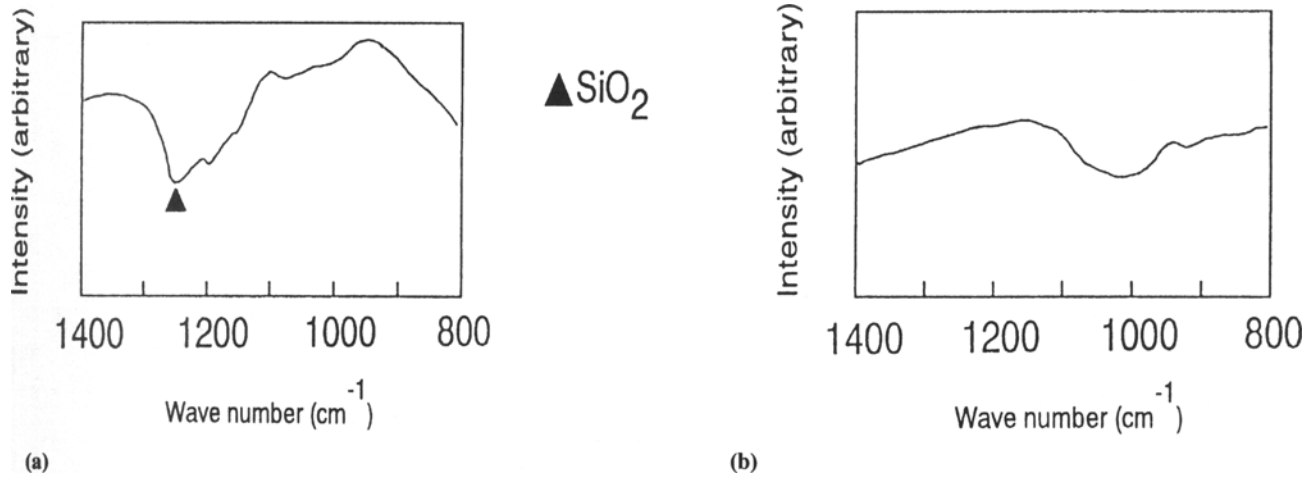


**Fig. 8** Infrared reflection spectra of the sample surface. (a) Infrared reflection spectra of the sample taken out in the middle of region III. (b) Infrared reflection spectra of the sample after the electrochemical measurement for 5 min

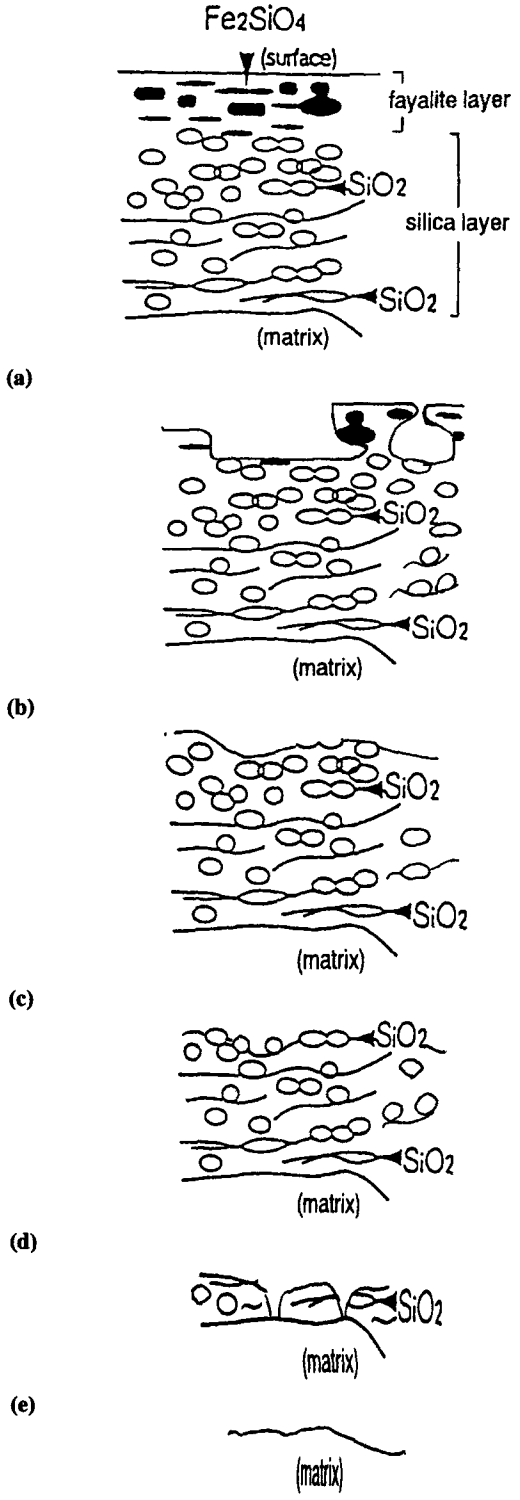


**Fig. 9** The correspondence between each region of time/voltage curve and each kind of internal oxide layer. (a) Initial state of internal oxide layers before electrochemical measurement. (b) The state of internal oxide layers taken out at the end of region I. (c) The state of internal oxide layers taken out at the end of region II. (d) The state of internal oxide layers taken out in the middle of region III. (e) The state of internal oxide layers taken out in the middle of region IV. (f) The state of sample taken out in the middle of region V

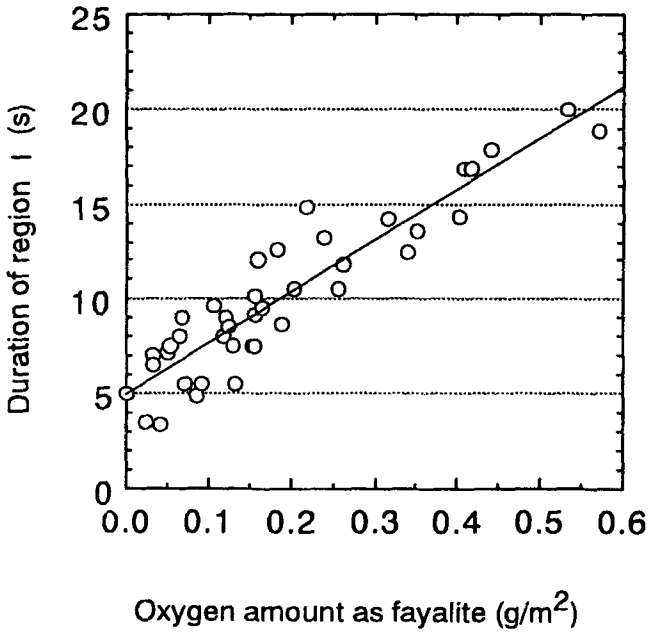


**Fig. 10** The relation between the oxygen amount as fayalite and the duration of region I

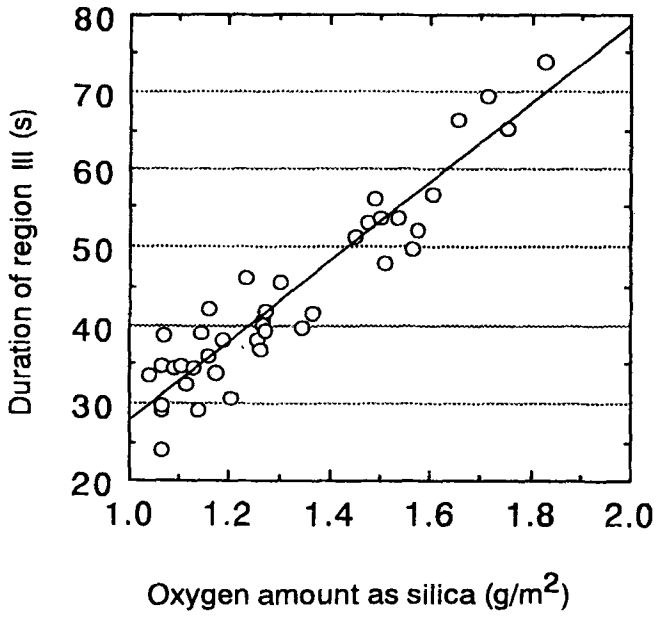


**Fig. 11** The relation between the oxygen amount as silica and the duration of region III

tents of fayalite and silica in the internal oxide layers can be easily obtained by this new method.

## 4. Conclusions

Characterization of internal oxide layers is possible by an electrochemical method. Specifically, the durations of regions

I and III obtained from a time/voltage curve correspond to the contents of fayalite and silica in the internal oxide layers, respectively.

## References


1. H. Ishitobi, B. Fukuda, and C. Kami, *CAMP-ISIJ,* Vol 5, 1992, p 1933
2. H. Ishitobi and C. Kami, *CAMP-ISIJ,* Vol 6, 1993, p 1829
3. S.D. Washko and W.G. Morris, *J. Magn. Mater.,* Vol 19, 1980, p 349
4. S.D. Washko and T.H. Shen, *J. Appl. Phys.,* Vol 53 (No. 11), 1982, p 8296
5. B. Fukuda, K. Sato, T. Ishida, Y. Itoh, and H. Shimanaka, *IEEE Trans. Magn.,* MAG-17, 1981, p 2878
6. Y. Hayakawa, M. Kurosawa, S. Keba, and M. Komatsubara, *CAMP-ISIJ,* Vol 3, 1990, p 1837
7. M. Komatsubara, Y. Hayakawa, M. Kurosawa, K. Iwamoto, and H. Ishitobi, *CAMP-ISIJ,* Vol 4, 1991, p 835
8. M. Watanabe, C. Kami, H. Ishitobi, and M. Komatsubara, *CAMP-ISIJ,* Vol 7, 1994, p 1819
9. A. Rahmel and J. Tobolski, *Werkst. Korros.,* Vol 16, 1965, p 662
10. N. Morito and T. Ichida, *Scr. Metall.,* Vol 10, 1976, p 619
11. N. Morito and T. Ichida, *Corros. Sci.,* Vol 17, 1977, p 961
12. W.F. Block and N. Jayaraman, *Mater. Sci. Technol.,* Vol 2, 1986, p 22